Generated using the official AMS LaTeX template v5.0

A Statistical Evaluation of WRF-LES Trace Gas Dispersion Using Project Prairie Grass Measurements

Alex Rybchuk*

Department of Mechanical Engineering, University of Colorado Boulder, Boulder CO, 80309

Caroline B. Alden

Cooperative Institute for Research in Environmental Sciences, University of Colorado Boulder, Boulder CO, 80309 and National Oceanic and Atmospheric Administration, Boulder, CO 80305

Julie K. Lundquist

Department of Atmospheric and Oceanic Sciences, University of Colorado Boulder, Boulder CO, 80309 and National Renewable Energy Laboratory, Golden CO, 80401

Gregory B. Rieker

Department of Mechanical Engineering, University of Colorado Boulder, Boulder CO, 80309

*Corresponding author: Alex Rybchuk, alex.rybchuk@colorado.edu

ABSTRACT

In recent years, new measurement systems have been deployed to monitor and quantify methane emissions from the natural gas sector. Large-eddy simulation (LES) has complemented measurement campaigns by serving as a controlled environment in which to study plume dynamics and sampling strategies. However, with few comparisons to controlled-release experiments, the accuracy of LES for modeling natural gas emissions is poorly characterized. In this paper, we evaluate LES from the Weather Research and Forecasting (WRF) model against measurements from the Project Prairie Grass campaign, surface layer similarity theory, and the Gaussian Plume Model. Using WRF-LES, we simulate continuous emissions from an ensemble of 30 near-surface trace gas sources in two stability regimes: strong and weak convection. We examine the impact of grid resolutions ranging from 6.25 m to 52 m in the horizontal dimension on model performance. We evaluate performance in a statistical framework, calculating fractional bias and conducting Welch's t-tests. WRF-LES accurately simulates observed surface concentrations at 100 m and beyond under strong convection; the magnitude of factional bias is less than 30% for the moderate- and fine-resolution simulations. However, in weakly convective conditions with strong winds, WRF-LES substantially overpredicts concentrations – the magnitude of fractional bias often exceeds 30%, and all but one t-test fails. Despite the good performance of dispersion in the strongly convective atmosphere, we find that both the strongly and weakly convective boundary layers disagree with empirical wind and temperature Monin-Obukhov similarity theory profiles that are often used to evaluate LES within the atmospheric surface layer.

1. Introduction

Natural gas production within the U.S. has surged in the past decade, increasing by more than 50% since 2010 (EIA 2020). Large emissions from routine operations (Thorpe et al. 2020) and malfunctioning equipment (Conley et al. 2016) have spurred the development of new methane emission monitoring instruments and platforms, including satellites, piloted aircraft, unmanned aircraft, open-path lasers, and ground-based point sensors (Fox et al. 2019). Source estimation techniques (SETs) are used to interpret source characteristics (e.g. emission rate) from the trace gas concentration measurements collected via these systems (Harper et al. 2011). Operational source estimation techniques (OSETs) are computationally low-cost and simple to use, and they vary from instrument to instrument. Satellites and remote sensing aircraft often use the integrated mass enhancement (IME) technique (Frankenberg et al. 2016; Varon et al. 2018; Jongaramrungruang et al. 2019). In situ aircraft measurements often use mass balance techniques (Karion et al. 2013; Conley et al. 2017). Many ground-based sensors employ techniques that rely on a transport and dispersion model, such as the Gaussian Plume Model (Pasquill 1972; U.S. EPA 2014; Coburn et al. 2018).

To build trust, OSETs are often tested and calibrated against measurements in the field. Of all the common OSETs used to quantify natural gas emissions, approaches based on the Gaussian Plume Model have been the most extensively tested against measurements. The Gaussian Plume Model has been evaluated and calibrated against hundreds of controlled releases through studies such as Project Prairie Grass (PPG) (Barad 1958) and the EPA OTM 33A evaluation study (U.S. EPA 2014). These studies have yielded better understanding of the accuracy and limitations of the Gaussian Plume Model for studying emissions from the natural gas sector. However, OSET evaluation studies that are based on measurements come with limitations, as they quantify performance in the specific conditions that are encountered in the field (e.g. atmospheric stability, terrain). For example, the OTM 33A evaluation study characterized performance in relatively flat terrain, but the technique has since been applied in hilly terrain (Caulton et al. 2019). Additionally, OSETs that rely on measurements from aircraft and satellites have been evaluated against fewer measurements. These techniques are newer, and it can be more expensive and logistically complicated to make measurements of controlled releases with these instruments. As a result, aircraft- and satellite-based OSETs have relied more heavily on synthetic observations from models, namely large-eddy simulation (LES). Overall, as new methods are developed to quantify methane emissions from the natural gas sector, it is critical to ensure that their corresponding OSETs are accurate.

Recently, interest has grown in using LES as a tool for studying natural gas emissions. LES is a computational approach that numerically solves the volume-averaged Navier-Stokes equations for flow at large scales and parameterizes small-scale flow with subgrid-scale models. It has been extensively applied in studies of the atmospheric boundary layer (ABL) (Deardorff 1972; Moeng 1984; Mason 1994; Beare et al. 2006). LES has been used as part of emission quantification studies to improve measurement strategies (Conley et al. 2017), evaluate and improve OSETs (Taylor et al. 2016; Varon et al. 2018), test new OSETs and their assumptions (Conley et al. 2017; Jongaramrungruang et al. 2019), generate realistic synthetic measurements of methane (Saide et al. 2018), and act as a transport model for field campaign observations (Caulton et al. 2018). LES is computationally expensive but offers several advantages over simpler gas transport and dispersion models. LES models the dynamic behavior of plumes as driven by time-varying winds, thereby circumventing the need to assume time-averaged fields or steady-state behavior, two assumptions employed in many simpler models. LES provides meteorological and concentration fields at all time steps and locations within a domain, whereas observations provide only a subset of these fields. LES can be used to used to study plume dynamics under desired atmospheric forcing, and furthermore, LES can simulate complicated physics encountered at real-world natural gas facilities, such as complex terrain (Lundquist et al. 2012; Xue et al. 2018) and time-varying emissions (Saide et al. 2018); therefore, in principle, LES could be used to accurately test OSETs or measurement strategies under a wide variety of environmental conditions.

Unfortunately, LES of atmospheric trace gas dispersion has been statistically evaluated against relatively few experimental measurements (Steinfeld et al. 2008; Ardeshiri et al. 2020), and thus its accuracy for emission quantification studies is not extensively characterized. The most well-known comparison studies focus on the strongly convective ABL in flat terrain. Convective tank studies first done by Willis and Deardorff (1976) and improved upon by Weil et al. (2002) provided a controlled environment to study tracer dispersion in strong convection. Additionally, the CONDORS study (Eberhard et al. 1988) released tracers into a real convective ABL. Subsequent LES studies have found good agreement with both sets of measurements in the mixed layer (Lamb 1978; Nieuwstadt and de Valk 1987; Weil et al. 2004, 2012; Nottrott et al. 2014).

LES evaluation studies that examine atmospheric dispersion in the surface layer (less than approximately 100 m above ground level) have often found worse performance. For example, Weil et al. (2012) compared surface concentrations in the atmospheric surface layer from an LES-driven Lagrangian particle dispersion model to observations from the PPG field campaign. The study found good agreement between the two beyond approximately 500 m downwind of the source, but LES underpredicted concentrations by as much as a factor of two 50 m downwind. Other studies suggest that LES dispersion underperforms when forced by conditions other than strong convection. In one neutral boundary layer, LES underpredicted horizontal trace gas dispersion (Nottrott et al. 2014). In a neutrally stratified field campaign study with multiple controlled releases, LES tended to overpredict emissions (Caulton et al. 2018). As many methane monitoring technologies measure within the atmospheric surface layer and in a range of atmospheric stabilities, understanding the performance of LES in these scenarios is key.

In this paper, we evaluate the performance of LES from the Weather Research and Forecasting model (WRF-LES) in the atmospheric surface layer under two types of forcing: strong convection and weak convection. We compare simulated surface concentrations from WRF-LES to data from the PPG field campaign, 50–800 m downwind of a passive tracer source. We assess the impact of LES grid resolution on plumes. Additionally, we compare against two well-studied transport and dispersion models that are often employed in ground-based OSETs: surface layer similarity (SLS) theory and the Gaussian Plume Model. Recognizing the importance of stochastic uncertainty caused by turbulence (Rao 2005), we evaluate performance in a statistical framework (Chang and Hanna 2004) and simulate a 30-member ensemble of plumes. In doing so, we aim to better understand the accuracy of WRF-LES under simple but realistic methane emission scenarios.

In Section 2, we describe the WRF-LES dispersion simulations, the PPG field campaign, the transport and dispersion models, and the statistical metrics used in this study. In Section 3, we evaluate the performance of WRF-LES in a strongly convective boundary layer, and we find good agreement with both measurements as well as SLS theory. In Section 4, we find that WRF-LES performance suffers in a weakly convective boundary layer. In Section 5, we discuss possible paths to improve LES accuracy, and we evaluate wind and temperature profiles relative to Monin-Obukhov similarity theory (MOST). In Section 6, we offer conclusions based on the study findings.

2. Methods

a. WRF-LES Simulations

We evaluate the performance of the LES code from Advanced Research WRF (WRF-ARW Version 4.1.2) (Skamarock et al. 2019). WRF-ARW is a numerical weather prediction code that uses the finite difference method to solve the compressible, nonhydrostatic Euler equations on a mass-based grid. It is a popular community-driven code with more than 36,000 registered users, and it serves as the foundation for several additional codes (Powers et al. 2017) with applications ranging from fire modeling (WRF-FIRE) to renewable energy modeling.

To evaluate the performance of WRF-LES, we simulate dispersion in the atmospheric boundary layer with six different configurations (Table 1). We model two types of convection—a strongly convective boundary layer (SCBL) and a weakly convective boundary layer (WCBL)—and we simulate each with a coarse-, moderate-, and fine-resolution grid. All cases incorporate flat terrain, cyclic boundary conditions for meteorological fields, a surface roughness of z_0 = 0.008 m, and homogeneous surface heating. Simulations are run without moisture, radiation, microphysics, or other parameterizations commonly employed in mesoscale WRF runs. The simulations in this study use third-order Runge-Kutta to step forward in time, as well as fifth-order horizontal advection and third-order vertical advection. The nonlinear backscatter anisotropic turbulence model captures subgrid effects (Kosović 1997; Mirocha et al. 2010), and MOST provides the lower boundary condition via the MM5 surface layer model (Jiménez et al. 2012).

Both the SCBL and WCBL spin up for two model hours, after which WRF begins to save the fields of interest. The SCBL is forced with constant 3.6 m s^{-1} geostrophic winds, 0.24 W K^{-1} m^{-1} surface heat flux, a 1 x 10^{-4} s^{-1} Coriolis parameter, and a 0.1-s time step. The SCBL horizontal grid resolutions are Δx = 52 m, 26 m, and 10 m for the coarse, moderate, and fine simulations, respectively. These forcings and the coarse grid resolution are consistent with Weil et al. (2012). The WCBL is forced with constant 10 m s^{-1} geostrophic winds, 0.1 W K^{-1} m^{-1} surface heat flux, a 1 x 10^{-4} s^{-1} Coriolis parameter, and a 0.05-s time step. The WCBL horizontal grid resolutions are 31.25, 15.625, and 6.25 m for the coarse, moderate, and fine simulations, respectively. All coarse and moderate simulations use constant vertical grid spacing, respectively 21 m and 10.5 m in the SCBL and 10.5 m and 5.25 m in the WCBL. The fine-resolution simulations use vertical grid resolutions that change. In the fine SCBL and WCBL simulations, the height of the first grid cell is $z_1 = 3$ m, and concentrations are output mid-cell height at 1.5 m. The near-surface grid cells stretch at a rate of 3% until $\Delta z = 10$ or 6.25 m is reached for the fine SCBL and WCBL respectively. Cells stretch again above the capping inversion at 3%, enabling higher resolution in the region area of interest at reduced computational expense.

To address the highly stochastic nature of dispersion in the turbulent ABL, continuous emissions are simulated from 30 different surface point sources in a grid with 500-m spacing, as in Weil et al. (2012) (Figure 1). Each source experiences different local winds, so that each plume evolves somewhat independently, circumventing the need for an ensemble of simulations for a single set of conditions. Each plume is tagged so that concentrations from one source are distinguishable from the other sources. Emissions are simulated from a point source at the lowest grid cell as in Nunalee et al. (2014). Dispersion is modeled in an Eulerian framework. As a result, the height of the emission source decreases as grid resolution is increased, which impacts concentrations nearest the source. To nullify the impact of recirculating plumes resulting from periodic boundary conditions, we include a trace gas absorbing plane 500 m upwind of each source.

After a two-hour spin-up, we sample trace gas fields and winds every second during a 10-minute period, matching the PPG measurement period. From these concentration fields, we calculate crosswind integrated concentration (CWIC) at a given radius as:

$$CWIC = \Delta s \left(\sum_i C_i \right), \tag{1}$$

where C_i is the concentration at a cell i and Δs is the arclength between cells. To account for the different release rates used in PPG, CWIC calculations throughout this study are normalized by emission rate Q, and this quantity is referred to as "concentration" though strictly speaking it is a "normalized crosswind integrated concentration". In order to compare the medium and coarse simulations to the PPG horizontal array measurements collected at a height of 1.5 m, concentration profiles are extrapolated using a 5th-order polynomial fit to concentrations in the lowest 100 m. For each simulated emission source, we calculate 10-minute-averaged CWIC at 50, 100, 200, 400, and 800 m downwind.

b. Project Prairie Grass

The PPG field campaign was conducted in 1956 in Kansas to study the near-surface behavior of passive tracer plumes during various meteorological conditions (Barad 1958). This campaign serves as a cornerstone for atmospheric dispersion models, informing key parameters in the Pasquill-Gifford stability classes for the Gaussian Plume Model (Venkatram 1996) and acting as a validation dataset for many regulatory dispersion models such as AERMOD (Cimorelli et al. 2005). Seventy controlled releases of SO_2 were carried out: six at 1.5 m above ground level and the remainder at 0.48 m. For each controlled release, 10-minute average concentration measurements were collected at an array of 599 individual sampling points. Measurements were conducted in concentric arcs 50, 100, 200, 400, and 800 m downwind of the release source. Along each arc, a horizontal array of point measurements was gathered at a height of 1.5 m, spaced 1° apart at 800 m and 2° at all other downwind distances. A vertical array of measurements was also collected 100 m downwind at heights 0.5, 1.0, 1.5, 2.5, 4.5, 7.5, 10.5, 13.5, and 17.5 m. The overall concentration uncertainties were reported as 1–2%. The roughness length of the site was estimated to be z_0 = 0.008 m (Sawford 2001). The winds employed in this study were measured with a cup anemometer 25 m west of the release source at a height of 2 m during a 10-minute period. Obukhov lengths L and friction velocities u_* were not directly measured during the campaign but were estimated from tower measurements in subsequent analysis (Horst et al. 1979). Normalized CWIC for the horizontal array is taken from Horst et al. (1979), and normalized CWIC for the vertical array is calculated using digitized data courtesy of www.harmo.org/jsirwin.

Measurements from a number of runs are either excluded in this analysis or not available. The runs used here are listed in Table 2. Data was not reported for Run 63 and Run 64 because of "extremely light and variable winds". Vertical tower measurements were gathered only for Run 13 and beyond and were additionally not reported for runs 23, 28, 35, 53, 63, and 64; thus, fewer vertical profiles are available for comparison. Winds speeds were not reported for Run 3 and Run 6, so those runs are excluded from this analysis.

We aim to compare as many observations to WRF-LES concentration simulations as possible. In principle, this comparison would best be achieved by running one simulation for each controlled release, because each release occurs in the presence of a different L and u_*; however, running one high-resolution simulation for each observation would be prohibitively expensive. As an alternative, we assess the performance of WRF-LES by binning PPG runs with similar atmospheric conditions into strongly convective and weakly convective categories. One common method to bin data in atmospheric dispersion studies is the Pasquill-Gifford stability classes (De Visscher 2013). These classes are traditionally delineated using wind speeds and solar radiation, but they can be alternatively delineated using a roughness length and Obukhov length (Golder 1972). Class A corresponds to $0 \geq L \geq -7$ m for the PPG roughness length. This range is used to bin PPG data for comparison with the SCBL LES runs, which have L between -6.1 and -5.4 m. The WCBL LES runs have L between -16 and -12.3 m, which falls on the border between Class B (-7 $\geq L \geq$ -15 m) and Class C stability (-15 $\geq L \geq$ -50 m). Accordingly, we use intermediate values of the PPG runs, -10 $\geq L \geq$ -35 m, for the LES WCBL comparison bin. To more closely resemble the WCBL LES, we additionally require $u_* \geq 0.4$ m s^{-1}.

c. Transport and Dispersion Models

We use two transport and dispersion models for comparison with the LES results: SLS theory and the Gaussian Plume Model.

SLS theory (van Ulden 1978) is used to complement the PPG observations. Each observation has a different pair of u_* and L values, and none of these pairs precisely match the conditions in the LES; however, SLS theory can be used to calculate approximate CWIC under any desired u_* and L conditions. Normalized CWIC at a height z is calculated for the PPG runs as:

$$\frac{CWIC(z)}{Q} = \frac{0.73}{\overline{u}\,\overline{z}} exp\left[-\left(\frac{0.66z}{\overline{z}}\right)^{1.5}\right], \tag{2}$$

where Q is the emission rate, $\overline{z}$ is the plume centerline height, and $\overline{u}$ is the wind speed at the plume centerline. The values of $\overline{z}$ and $\overline{u}$ are numerically computed based on MOST, and downwind distance x is implicitly a function of these variables. SLS theory is strictly valid for releases at a height of 0 m, but it agrees well with the observations in this study (Appendix). As such, we use SLS theory as a proxy for hypothetical observations, with u_* and L that match those of the LES.

Although SLS theory cannot be used to directly study the sensitivity of dispersion to source height and wind speed, the Gaussian Plume Model does approximate how dispersion responds to these two factors. Normalized CWIC at downwind distance x and height z is calculated for the SCBL with the Gaussian Plume Model (Arya 1999):

$$\frac{CWIC(x,z)}{Q} = \frac{1}{\sqrt{2\pi} u \sigma_z}\left[exp\left(-\frac{(z-h)^2}{2\sigma_z^2}\right) + exp\left(-\frac{(z+h)^2}{2\sigma_z^2}\right)\right], \tag{3}$$

where u is the wind speed at the source, σ_z is the vertical plume spread, and h is the emission height, assumed to be 0.48 m. The Briggs (1973) equations are used to calculate σ_z, where Pasquill-Gifford Class A is employed.

d. Statistical Metrics

Chang and Hanna (2004) summarize metrics for evaluating dispersion models by comparing an observation, C_o, to a model prediction, C_p. While there is no one optimal metric, they conclude that "good performing models" have predictions that fall within a factor 2 of observations (FAC2) at least 50% of the time, that the relative mean bias (here fractional bias, FB) is less than 30%, and that the relative scatter (here normalized mean square error, NMSE) is less than approximately a factor of two. FAC2 is calculated as the fraction of data within $0.5 \leq C_p/C_o \leq 2.0$. Fractional bias is calculated as:

$$FB = \frac{\overline{C}_o - \overline{C}_p}{2(\overline{C}_o + \overline{C}_p)}, \tag{4}$$

where averages are taken over the set of measurements or simulations. NMSE is calculated as:

$$NMSE = \frac{\overline{(C_o - C_p)^2}}{\overline{C}_o \overline{C}_p}. \tag{5}$$

Here, only observations for the horizontal array are used for quantitative comparison, as the vertical array stability bins have only two or three observations.

SLS model performance is compared against observations using FAC2, FB, and NMSE (Appendix). In contrast, FAC2 and NMSE are not calculated for LES because these metrics require each observation to be paired with a model prediction. Instead, we use the Welch's t-test to compare the LES distribution and the observed distribution of concentration. Both distributions are assumed to be Gaussian at each downwind location. The null hypothesis is that the mean concentrations for these distributions are identical, and the test is conducted at the 95% confidence interval with a two-sided tail. Mean LES concentrations are also evaluated using FB. However, for the FB comparison, SLS theory serves as comparison—instead of observations—in order to minimize error stemming from differences in L and u_*.

3. Evaluation of LES in the Strongly Convective Boundary Layer

a. Horizontal Surface Concentrations

LES of trace gas plumes in the SCBL performs well from the perspective of grid convergence (Figure 2). Mean surface concentrations in the coarse-, moderate-, and fine-resolution simulations collapse onto the same line beyond 200 m; however, LES surface concentrations upwind of 200 m increase as resolution is increased, suggesting that concentrations are grid-dependent close to the source. For example, at 50 m downwind (Figure 2 inset), the fine simulation concentrations exceed those from the coarse simulation by a factor of 1.6. This increase may be attributable to two factors that change with resolution in the lowest grid cell: emission height and wind speed. As vertical resolution increases, the simulated emission height decreases from 10.5 m in the coarse simulation to 1.5 m in the fine simulation, as trace gas is released from the center of the lowest cell. A lower emission height leads to higher surface concentrations near the source. This change in resolution also leads to slower wind speeds in the lowest grid cell, due to the increased proximity to the surface. The winds in the lowest grid cell of the fine-resolution simulation $u_{h=1.5,fine} = 1.16$ m s^{-1} are slower than those in the lowest grid cell of the coarse simulation $u_{h=10,coarse} = 1.92$ m

s^{-1}. Slower winds lead to less plume dispersion and therefore higher concentrations at the same downwind distance.

We employ the Gaussian Plume Model to quantitatively estimate the impact of these two factors. Using Equation 3, CWIC is calculated at 50 m for emission heights of 1.5 and 10.5 m, both driven by fine winds $u_{h=1.5,fine}$. The concentration from the 1.5-m release exceeds that from the 10.5-m height release by a factor of 1.6. We also calculate 50-m CWIC for $u_{h=1.5,fine}$ winds and $u_{h=10,coarse}$ winds at the same release height of 1.5 m. This change in wind speeds also leads to a factor 1.6 increase in concentrations at higher wind speeds. Taken together, the Gaussian Plume Model predicts that a change in source height and wind speed would lead to a factor 2.6 increase in 50-m CWIC. This increase is larger than the observed factor 1.6 increase between the fine and coarse LES. Nonetheless, we conclude that both factors contribute roughly equally to a near-source increase in concentrations as grid resolution is refined.

LES of the SCBL also performs well relative to observations. Beyond 200 m downwind, all LES resolutions show good fractional bias (|FB| < 30%) relative to SLS (Table 3). This behavior is consistent with Weil et al. (2012), who studied dispersion in identical SCBL conditions with Lagrangian particle dispersion driven by a different LES code, NCAR-LES. As WRF-LES resolution increases, performance improves close to the source. FB at 100 m decreases from 40% to 15%, and FB at 50 m decreases from 78% to 38% when moving from the coarse to the fine simulation.

A Welch's t-test at each downwind location is used to assess whether the average LES and average measured concentrations differ significantly. The t-test results corroborate the FB findings. More than 200 m downwind of the source, all LES resolutions produce concentration distributions whose mean concentrations are statistically indistinguishable from those of PPG. Closer to the source, resolution plays an increasingly important role. The coarse resolution simulation fails the t-test at 100 m, but the moderate- and fine-resolution cases succeed.

It is crucial that these comparisons are rooted in a statistical framework—LES ensemble members in the SCBL display a significant amount of scatter. At 200 m and beyond, the minimum and maximum concentrations differ by more than an order of magnitude. This scatter occurs even though all plumes are subject to the same geostrophic winds and surface heating. In the SCBL, individual plume behavior is strongly governed by the local presence of updrafts and downdrafts (Weil et al. 2012).

b. Vertical Concentration Profiles

As with the horizontal array, we find that WRF-LES performs well against vertical profiles of concentration (Figure 3). The average concentrations agree for the coarse-, moderate-, and fine-resolution simulations at heights above 10.5 m, which is the height of the lowest concentration measurement from the coarse simulation. The coarse simulation predicts relatively narrow variability between ensemble members, but the moderate- and fine-resolution simulation have similar spread to each other. WRF-LES agrees well with SLS theory and shows only minor deviations at 17.5 m, which may be attributed to differing micrometeorological conditions. The PPG observations show a slightly stronger concentration gradient across the surface layer, but this difference may also be attributable to different values of L and u_*. In the SCBL, LES qualitatively performs well against surface concentrations as well as vertical profiles at 100 m.; thus in conjunction with the analysis of the horizontal array, we conclude that WRF-LES accurately models realistic plume behavior in the SCBL, provided sufficient resolution is used.

4. Evaluation of LES in the Weakly Convective Boundary Layer

a. Horizontal Surface Concentrations

Unlike the SCBL, the LES simulations of the WCBL perform poorly relative to SLS theory and observations in the horizontal dimension (Table 4). Most comparisons show |FB| > 30%, which is outside the "good" performance threshold from Chang and Hanna (2004). While |FB| < 30% near 100 m, this downwind distance is simply the crossover point where LES transitions from overprediction to underprediction. Additionally, every comparison aside from the 200-m coarse resolution case fails the t-test. This single success case is dismissed as coincidental, because the 200-m results turn to "Reject" when grid resolution is increased.

b. Vertical Concentration Profiles

The WCBL similarly performs poorly relative to the vertical array of measurements (Figure 5). Profiles of concentration do not converge as well across different resolutions in the WCBL as in the SCBL. The mean LES concentrations for the moderate- and fine-resolution simulations agree above 10 m but show different behavior below. Interestingly, the moderate resolution simulations show substantially less scatter than both the coarse and the fine simulations, further underscoring the lack of grid convergence. Furthermore, LES substantially overpredicts concentrations relative to both observations and SLS theory. Altogether, WRF-LES performs poorly in the weakly convective case.

5. Discussion on Disagreement in the WCBL

Near-surface turbulence within the atmospheric surface layer is characterized by anisotropy, a small outer length scale, a strong dependence on atmospheric stability, and a "reverse turbulent cascade" where small scales transfer energy to larger scales (Sullivan et al. 2003). These characteristics make it challenging for LES to accurately model flow in this region, and the inability of our LES to capture all of these features likely drives the overpredicted concentrations in the WCBL. Modelers are actively researching methods to improve LES accuracy near solid surfaces. Within the atmospheric surface layer, these techniques include improving subgrid-scale models (Porté-Agel et al. 2000; Bou-Zeid et al. 2005; Chung and Matheou 2014; Mokhtarpoor and Heinz 2017), improving wall models (Maronga et al. 2019), and refining grid size and aspect ratio (Brasseur and Wei 2010; Daniels et al. 2016).

During their development, LES techniques for the surface layer are typically evaluated against MOST. This theory is derived for flat terrain under homogeneous forcing, as is the case in this LES study, and it has been shown to agree well with observations in these conditions (Businger et al. 1971; Dyer 1974). MOST describes wind and temperature profiles in the atmospheric surface layer based on L; a non-dimensional wind shear, ϕ_m; and a non-dimensional temperature gradient, ϕ_h (Stull 1988). This non-dimensional function takes one of many similar empirical forms (Maronga and Reuder 2017), and it is calculated from either observations or LES as

$$\phi_m\left(\frac{z}{L}\right) = \frac{d\overline{u}_h}{dz}\frac{\kappa z}{u_*}, \text{ and} \tag{6}$$

$$\phi_h\left(\frac{z}{L}\right) = \frac{d\overline{\theta}}{dz}\frac{\kappa z}{\theta_*}, \tag{7}$$

where $\overline{u}_h$ is the mean horizontal wind speed, $\overline{\theta}$ is the average potential temperature, θ_* is the kinematic heat flux divided by friction velocity, and κ is the von Kármán constant, taken to be 0.4.

We calculate ϕ_m directly from LES wind fields and compare it to empirical profiles based on the LES values of u_* and L using the Dyer (1974) equations (Figure 6 a,b). At all three resolutions, the LES-based non-dimensional wind shear profiles in the SCBL agree well with one another. These profiles are larger than the empirical MOST profile by about a factor of two, but they all qualitatively show similar behavior. On the other hand, the ϕ_m profiles in the WCBL behave differently. A large peak ("overshoot") is observed in the LES-based profiles, and the height of this overshoot decreases as resolution increases, as in Brasseur and Wei (2010). We similarly calculate ϕ_h profiles (Figure 6 c,d). All LES-based profiles show dependence on grid resolution as well as an overshoot both within the SCBL and in the WCBL. Interestingly, this overshoot is larger within the SCBL even though no overshoot was observed in its corresponding wind shear profiles.

These profiles illuminate an interesting discrepancy between using PPG observations and using MOST to diagnose LES performance. LES of the WCBL agrees poorly with the PPG trace gas observations; thus, the LES-based MOST profiles unsurprisingly agree poorly with their anticipated form. At the same time however, LES of the SCBL agrees well with PPG while simultaneously disagreeing with MOST profiles. This inconsistency suggests one of two scenarios: that either the geostropic wind and the heat flux selected for the SCBL LES were coincidentally good choices or that LES can accurately resolve near-surface dispersion under certain conditions even if it disagrees with MOST. For example, perhaps the lack of a wind shear overshoot in the SCBL explains its good dispersion performance. Future LES studies of near-surface dispersion will clarify which case is true.

6. Conclusion

In this study, we assess the accuracy of WRF-LES for simulating trace gas dispersion in three strongly convective and three weakly convective boundary layers where grid resolution is varied. We compare 30 plumes within each simulation to horizontal and vertical measurements from the Project Prairie Grass campaign (50–800 m downwind of a source, with measurements at heights of 0.5–17.5 m). We also compare WRF-LES simulations to surface layer similarity theory and the Gaussian Plume Model. We evaluate the performance of WRF-LES dispersion using a statistical framework, relying on the fractional bias metric and Welch's t-tests to compare distributions. In strongly convective conditions with weak winds, WRF-LES, the Project Prairie Grass measurements, and the SLS theory tend to agree well. Furthermore, WRF-LES performs better as grid resolution is increased. In contrast, during weak convection and stronger winds, WRF-LES substantially overpredicts concentrations.

To shed more light on the performance of LES within the lower atmospheric surface layer, we evaluate wind and temperature profiles against Monin-Obukhov similarity theory (MOST). We find that the weakly convective LES poorly agrees with MOST, which may justify the poor performance of dispersion under this forcing; however, we simultaneously find that LES of the strongly convective boundary layer also disagrees with MOST, even though the simulated concentrations agree with Project Prairie Grass measurements. We suggest further study on the relationship between wind, temperature, and trace gas concentration for LES of the atmospheric surface layer.

The results of this study caution that WRF-LES, and atmospheric LES codes in general, should be evaluated in a statistical framework to available empirical datasets when possible. By simulating 30 plumes under identical large-scale forcing, we consider the stochastic nature of turbulent diffusion. At times we observe order-of-magnitude differences in 10-minute averaged concentrations. This study examined the simple case of flat terrain and homogeneous forcing, but the conclusions are broadly applicable to studies examining dispersion in more challenging scenarios, such as complex terrain or urban environments.

LES has many unique features, which makes it an invaluable tool for modeling emissions of trace gases. LES can be, and has been used, to improve measurement strategies for field campaigns. It can simulate dispersion in complex environments, which is valuable as regulators seek to characterize real-world emissions in industrial environments with complex terrain and time-varying emissions. Through further comparisons against controlled releases, trust in LES dispersion can be fostered, and it can begin to take a more central role in the emission quantification challenge.

Acknowledgments. We thank Ian Faloona, Branko Kosović, and Jeffery C. Weil for their insight while preparing this manuscript. AR, CA, and GR were supported by a grant from the Department of Energy, Office of Fossil Energy, National Energy Technology Laboratory (DE- FE0029168). The simulations here were conducted with supercomputing resources from the University of Colorado Boulder Research Computing Group, which is supported by the National Science Foundation (awards ACI-1532235 and ACI-1532236), the University of Colorado Boulder, and Colorado State University. This work was authored in part by the National Renewable Energy Laboratory, operated by Alliance for Sustainable Energy, LLC, for the U.S. Department of Energy (DOE) under Contract No. DE-AC36-08GO28308. Funding provided by the U.S. Department of Energy Office of Energy Efficiency and Renewable Energy Wind Energy Technologies Office. The views expressed in the article do not necessarily represent the views of the DOE or the U.S. Government. The U.S. Government retains and the publisher, by accepting the article for publication, acknowledges that the U.S. Government retains a nonexclusive, paid-up, irrevocable, worldwide license to publish or reproduce the published form of this work, or allow others to do so, for U.S. Government purposes.

Data availability statement. The namelists and 3D 10-minute time-averaged WRF-LES meteorological and plume fields used in this study can be found at https://doi.org/10.5281/zenodo.3909881. The digitized Project Prairie Grass measurements were provided courtesy of www.harmo.org/jsirwin.

References

Ardeshiri, H., M. Cassiani, S. Y. Park, A. Stohl, I. Pisso, and A. S. Dinger, 2020: On the Convergence and Capability of the Large-Eddy Simulation of Concentration Fluctuations in Passive Plumes for a Neutral Boundary Layer at Infinite Reynolds Number. *Boundary-Layer Meteorol*, doi:10.1007/s10546-020-00537-6, URL https://doi.org/10.1007/s10546-020-00537-6.

Arya, S. P., 1999: *Air pollution meteorology and dispersion*. Oxford University Press.

Barad, M. L., 1958: Project Prairie Grass, A Field Program in Diffusion, Volume I. Tech. rep.

Beare, R. J., and Coauthors, 2006: An Intercomparison of Large-Eddy Simulations of the Stable Boundary Layer. *Boundary-Layer Meteorology*, **118 (2)**, 247–272, doi:10.1007/s10546-004-2820-6, URL http://link.springer.com/10.1007/s10546-004-2820-6.

Bou-Zeid, E., C. Meneveau, and M. Parlange, 2005: A scale-dependent Lagrangian dynamic model for large eddy simulation of complex turbulent flows. *Physics of Fluids*, **17 (2)**, 025 105, doi:10.1063/1.1839152, URL https://aip.scitation.org/doi/full/10.1063/1.1839152.

Brasseur, J. G., and T. Wei, 2010: Designing large-eddy simulation of the turbulent boundary layer to capture law-of-the-wall scaling. *Physics of Fluids*, **22 (2)**, 021 303, doi:10.1063/1.3319073, URL https://aip.scitation.org/doi/full/10.1063/1.3319073.

Briggs, G. A., 1973: Diffusion Estimation for Small Emissions. Atmospheric Turbulence and Diffusion Laboratory, NOAA.

Businger, J. A., J. C. Wyngaard, Y. Izumi, and E. F. Bradley, 1971: Flux-Profile Relationships in the Atmospheric Surface Layer. *J. Atmos. Sci.*, **28 (2)**, 181–189, doi: 10.1175/1520-0469(1971)028<0181:FPRITA>2.0.CO;2, URL https://journals.ametsoc.org/

doi/10.1175/1520-0469%281971%29028%3C0181%3AFPRITA%3E2.0.CO%3B2, publisher: American Meteorological Society.

Caulton, D. R., and Coauthors, 2018: Quantifying uncertainties from mobile-laboratory-derived emissions of well pads using inverse Gaussian methods. *Atmospheric Chemistry and Physics*, **18 (20)**, 15 145–15 168, doi:10.5194/acp-18-15145-2018, URL https://www.atmos-chem-phys.net/18/15145/2018/.

Caulton, D. R., and Coauthors, 2019: Importance of Superemitter Natural Gas Well Pads in the Marcellus Shale. *Environ. Sci. Technol.*, **53 (9)**, 4747–4754, doi:10.1021/acs.est.8b06965, URL https://doi.org/10.1021/acs.est.8b06965, publisher: American Chemical Society.

Chang, J. C., and S. R. Hanna, 2004: Air quality model performance evaluation. *Meteorol Atmos Phys*, **87 (1-3)**, doi:10.1007/s00703-003-0070-7, URL http://link.springer.com/10.1007/s00703-003-0070-7.

Chung, D., and G. Matheou, 2014: Large-Eddy Simulation of Stratified Turbulence. Part I: A Vortex-Based Subgrid-Scale Model. *J. Atmos. Sci.*, **71 (5)**, 1863–1879, doi:10.1175/JAS-D-13-0126.1, URL https://journals.ametsoc.org/doi/full/10.1175/JAS-D-13-0126.1.

Cimorelli, A. J., and Coauthors, 2005: AERMOD: A Dispersion Model for Industrial Source Applications. Part I: General Model Formulation and Boundary Layer Characterization. *J. Appl. Meteor.*, **44 (5)**, 682–693, doi:10.1175/JAM2227.1, URL https://journals.ametsoc.org/jamc/article/44/5/682/16648/AERMOD-A-Dispersion-Model-for-Industrial-Source, publisher: American Meteorological Society.

Coburn, S., and Coauthors, 2018: Regional trace-gas source attribution using a field-deployed dual frequency comb spectrometer. *Optica*, **5 (4)**, 320, doi:10.1364/OPTICA.5.000320, URL https://www.osapublishing.org/abstract.cfm?URI=optica-5-4-320.

Conley, S., G. Franco, I. Faloona, D. R. Blake, J. Peischl, and T. B. Ryerson, 2016: Methane emissions from the 2015 Aliso Canyon blowout in Los Angeles, CA. *Science*, **351 (6279)**, 1317–1320, doi:10.1126/science.aaf2348, URL https://science.sciencemag.org/content/351/6279/1317, publisher: American Association for the Advancement of Science Section: Report.

Conley, S., and Coauthors, 2017: Application of Gauss's theorem to quantify localized surface emissions from airborne measurements of wind and trace gases. *Atmospheric Measurement Techniques; Katlenburg-Lindau*, **10 (9)**, 3345–3358, doi:http://dx.doi.org/10.5194/amt-10-3345-2017, URL https://search.proquest.com/docview/1938022483/abstract/DD3E23751CB549A6PQ/1.

Daniels, M. H., K. A. Lundquist, J. D. Mirocha, D. J. Wiersema, and F. K. Chow, 2016: A New Vertical Grid Nesting Capability in the Weather Research and Forecasting (WRF) Model. *Mon. Wea. Rev.*, **144 (10)**, 3725–3747, doi:10.1175/MWR-D-16-0049.1, URL http://journals.ametsoc.org/doi/10.1175/MWR-D-16-0049.1.

De Visscher, A., 2013: *Air Dispersion Modeling : Foundations and Applications*. John Wiley & Sons, Incorporated, 2013.

Deardorff, J. W., 1972: Numerical Investigation of Neutral and Unstable Planetary Boundary Layers. *J. Atmos. Sci.*, **29 (1)**, 91–115, doi:10.1175/1520-0469(1972)029<0091:NIONAU>2.0.CO;2, URL https://journals.ametsoc.org/jas/article/29/1/91/18079/Numerical-Investigation-of-Neutral-and-Unstable, publisher: American Meteorological Society.

Dyer, A. J., 1974: A review of flux-profile relationships. *Boundary-Layer Meteorol*, **7 (3)**, 363–372, doi:10.1007/BF00240838, URL https://doi.org/10.1007/BF00240838.

Eberhard, W. L., W. R. Moninger, and G. A. Briggs, 1988: Plume Dispersion in the Convective Boundary Layer. Part I: CONDORS Field Experiment and Example Measurements. *J. Appl. Meteor.*, **27 (5)**, 599–616, doi:10.1175/1520-0450(1988)027<0599:PDITCB>2.0.CO;2, URL https://journals.ametsoc.org/jamc/article/27/5/599/14420/Plume-Dispersion-in-the-Convective-Boundary-Layer, publisher: American Meteorological Society.

EIA, 2020: United States dry natural gas production. accessed 22 june 2020. URL https://www.eia.gov/dnav/ng/hist/n9070us2A.htm.

Fox, T. A., T. E. Barchyn, D. Risk, A. P. Ravikumar, and C. H. Hugenholtz, 2019: A review of close-range and screening technologies for measuring fugitive methane emissions in upstream oil and gas. *Environmental Research Letters*, doi:10.1088/1748-9326/ab0cc3, URL http://iopscience.iop.org/article/10.1088/1748-9326/ab0cc3.

Frankenberg, C., and Coauthors, 2016: Airborne methane remote measurements reveal heavy-tail flux distribution in Four Corners region. *Proc Natl Acad Sci USA*, **113 (35)**, 9734–9739, doi:10.1073/pnas.1605617113, URL http://www.pnas.org/lookup/doi/10.1073/pnas.1605617113.

Golder, D., 1972: Relations among stability parameters in the surface layer. *Boundary-Layer Meteorol*, **3 (1)**, 47–58, doi:10.1007/BF00769106, URL https://doi.org/10.1007/BF00769106.

Harper, L. A., O. T. Denmead, and T. K. Flesch, 2011: Micrometeorological techniques for measurement of enteric greenhouse gas emissions. *Animal Feed Science and Technology*,

166-167, 227–239, doi:10.1016/j.anifeedsci.2011.04.013, URL http://www.sciencedirect.com/science/article/pii/S0377840111001325.

Horst, T. W., J. C. Doran, and P. W. Nickola, 1979: Evaluation of empirical atmospheric diffusion data. URL https://digital.library.unt.edu/ark:/67531/metadc1091573/m1/1/, doi:10.2172/5716471.

Jiménez, P. A., J. Dudhia, J. F. González-Rouco, J. Navarro, J. P. Montávez, and E. García-Bustamante, 2012: A Revised Scheme for the WRF Surface Layer Formulation. *Mon. Wea. Rev.*, **140 (3)**, 898–918, doi:10.1175/MWR-D-11-00056.1, URL https://journals.ametsoc.org/mwr/article/140/3/898/104000/A-Revised-Scheme-for-the-WRF-Surface-Layer, publisher: American Meteorological Society.

Jongaramrungruang, S., C. Frankenberg, G. Matheou, A. K. Thorpe, D. R. Thompson, L. Kuai, and R. M. Duren, 2019: Towards accurate methane point-source quantification from high-resolution 2-D plume imagery. *Atmospheric Measurement Techniques*, **12 (12)**, 6667–6681, doi:https://doi.org/10.5194/amt-12-6667-2019, URL https://www.atmos-meas-tech.net/12/6667/2019/.

Karion, A., and Coauthors, 2013: Methane emissions estimate from airborne measurements over a western United States natural gas field. *Geophysical Research Letters*, **40 (16)**, 4393–4397, doi:10.1002/grl.50811, URL https://agupubs.onlinelibrary.wiley.com/doi/abs/10.1002/grl.50811.

Kosović, B., 1997: Subgrid-scale modelling for the large-eddy simulation of high-Reynolds-number boundary layers. *Journal of Fluid Mechanics*, **336**, 151–182, doi:10.1017/S0022112096004697, URL https://www.cambridge.org/core/journals/journal-of-fluid-mechanics/article/subgridscale-modelling-for-the-largeeddy-simulation-of-highreynoldsnumber-boundary-layers/F28B6A44C9DE53830111229D995C09ED.

Lamb, R. G., 1978: A numerical simulation of dispersion from an elevated point source in the convective planetary boundary layer. *Atmospheric Environment (1967)*, **12 (6)**, 1297–1304, doi:10.1016/0004-6981(78)90068-9, URL http://www.sciencedirect.com/science/article/pii/0004698178900689.

Lundquist, K. A., F. K. Chow, and J. K. Lundquist, 2012: An Immersed Boundary Method Enabling Large-Eddy Simulations of Flow over Complex Terrain in the WRF Model. *Mon. Wea. Rev.*, **140 (12)**, 3936–3955, doi:10.1175/MWR-D-11-00311.1, URL https://journals.ametsoc.org/doi/full/10.1175/MWR-D-11-00311.1.

Maronga, B., C. Knigge, and S. Raasch, 2019: An Improved Surface Boundary Condition for Large-Eddy Simulations Based on Monin–Obukhov Similarity Theory: Evaluation and Consequences for Grid Convergence in Neutral and Stable Conditions. *Boundary-Layer Meteorol*, doi:10.1007/s10546-019-00485-w, URL https://doi.org/10.1007/s10546-019-00485-w.

Maronga, B., and J. Reuder, 2017: On the Formulation and Universality of Monin–Obukhov Similarity Functions for Mean Gradients and Standard Deviations in the Unstable Surface Layer: Results from Surface-Layer-Resolving Large-Eddy Simulations. *J. Atmos. Sci.*, **74 (4)**, 989–1010, doi:10.1175/JAS-D-16-0186.1, URL https://journals.ametsoc.org/doi/full/10.1175/JAS-D-16-0186.1.

Mason, P. J., 1994: Large-eddy simulation: A critical review of the technique. *Quarterly Journal of the Royal Meteorological Society*, **120 (515)**, 1–26, doi:10.1002/qj.49712051503, URL https://rmets.onlinelibrary.wiley.com/doi/abs/10.1002/qj.49712051503, _eprint: https://rmets.onlinelibrary.wiley.com/doi/pdf/10.1002/qj.49712051503.

Mirocha, J. D., J. K. Lundquist, and B. Kosović, 2010: Implementation of a Nonlinear Subfilter Turbulence Stress Model for Large-Eddy Simulation in the Advanced Research WRF Model.

Mon. Wea. Rev., **138 (11)**, 4212–4228, doi:10.1175/2010MWR3286.1, URL http://journals.ametsoc.org/doi/abs/10.1175/2010MWR3286.1.

Moeng, C.-H., 1984: A Large-Eddy-Simulation Model for the Study of Planetary Boundary-Layer Turbulence. *J. Atmos. Sci.*, **41 (13)**, 2052–2062, doi:10.1175/1520-0469(1984)041<2052:ALESMF>2.0.CO;2, URL https://journals.ametsoc.org/jas/article/41/13/2052/20986/A-Large-Eddy-Simulation-Model-for-the-Study-of, publisher: American Meteorological Society.

Mokhtarpoor, R., and S. Heinz, 2017: Dynamic large eddy simulation: Stability via realizability. *Physics of Fluids*, **29 (10)**, 105 104, doi:10.1063/1.4986890, URL https://aip.scitation.org/doi/full/10.1063/1.4986890.

Nieuwstadt, F. T. M., and J. P. J. M. M. de Valk, 1987: A large eddy simulation of buoyant and non-buoyant plume dispersion in the atmospheric boundary layer. *Atmospheric Environment (1967)*, **21 (12)**, 2573–2587, doi:10.1016/0004-6981(87)90189-2, URL http://www.sciencedirect.com/science/article/pii/0004698187901892.

Nottrott, A., J. Kleissl, and R. Keeling, 2014: Modeling passive scalar dispersion in the atmospheric boundary layer with WRF large-eddy simulation. *Atmospheric Environment*, **82**, 172–182, doi:10.1016/j.atmosenv.2013.10.026, URL http://www.sciencedirect.com/science/article/pii/S1352231013007796.

Nunalee, C. G., B. Kosović, and P. E. Bieringer, 2014: Eulerian dispersion modeling with WRF-LES of plume impingement in neutrally and stably stratified turbulent boundary layers. *Atmospheric Environment*, **99**, 571–581, doi:10.1016/j.atmosenv.2014.09.070, URL http://www.sciencedirect.com/science/article/pii/S1352231014007638.

Pasquill, F., 1972: Some aspects of boundary layer description. *Quarterly Journal of the Royal Meteorological Society*, **98 (417)**, 469–494, doi:10.1002/qj.49709841702, URL http://rmets.onlinelibrary.wiley.com/doi/abs/10.1002/qj.49709841702, _eprint: https://onlinelibrary.wiley.com/doi/pdf/10.1002/qj.49709841702.

Porté-Agel, F., C. Meneveau, and M. B. Parlange, 2000: A scale-dependent dynamic model for large-eddy simulation: application to a neutral atmospheric boundary layer. *Journal of Fluid Mechanics*, **415**, 261–284, doi:10.1017/S0022112000008776, URL https://www.cambridge.org/core/journals/journal-of-fluid-mechanics/article/scaledependent-dynamic-model-for-largeeddy-simulation-application-to-a-neutral-atmospheric-boundar 34CEC8EC0190725FE5C0648D8022F374, publisher: Cambridge University Press.

Powers, J. G., and Coauthors, 2017: The Weather Research and Forecasting Model: Overview, System Efforts, and Future Directions. *Bull. Amer. Meteor. Soc.*, **98 (8)**, 1717–1737, doi:10.1175/BAMS-D-15-00308.1, URL https://journals.ametsoc.org/bams/article/98/8/1717/216092/The-Weather-Research-and-Forecasting-Model, publisher: American Meteorological Society.

Rao, K. S., 2005: Uncertainty Analysis in Atmospheric Dispersion Modeling. *Pure and Applied Geophysics*, **162 (10)**, 1893–1917, doi:10.1007/s00024-005-2697-4, URL http://link.springer.com/10.1007/s00024-005-2697-4.

Saide, P. E., D. Steinhoff, B. Kosovic, J. Weil, N. Downey, D. Blewitt, S. Hanna, and L. Delle Monache, 2018: Evaluating methods to estimate methane emissions from oil and gas production facilities using LES simulations. *Environ. Sci. Technol.*, doi:10.1021/acs.est.8b01767, URL https://doi.org/10.1021/acs.est.8b01767.

Sawford, B. L., 2001: Project Prairie Grass - a Classic Atmospheric Dispersion Experiment Revisited. *14th Australasian Fluid Mechanics Conference*, Adelaide University, Adelaide, Australia.

Skamarock, W. C., and Coauthors, 2019: A Description of the Advanced Research WRF Model Version 4. 162.

Steinfeld, G., S. Raasch, and T. Markkanen, 2008: Footprints in Homogeneously and Heterogeneously Driven Boundary Layers Derived from a Lagrangian Stochastic Particle Model Embedded into Large-Eddy Simulation. *Boundary-Layer Meteorol*, **129 (2)**, 225–248, doi:10.1007/s10546-008-9317-7, URL https://link.springer.com/article/10.1007/s10546-008-9317-7.

Stull, R. B., 1988: *An Introduction to Boundary Layer Meteorology*. Kluwer.

Sullivan, P. P., T. W. Horst, D. H. Lenschow, C.-H. Moeng, and J. C. Weil, 2003: Structure of subfilter-scale fluxes in the atmospheric surface layer with application to large-eddy simulation modelling. *J. Fluid Mech.*, **482**, 101–139, doi:10.1017/S0022112003004099, URL http://www.journals.cambridge.org/abstract_S0022112003004099.

Taylor, D. M., F. K. Chow, M. Delkash, and P. T. Imhoff, 2016: Numerical simulations to assess the tracer dilution method for measurement of landfill methane emissions. *Waste Management*, **56**, 298–309, doi:10.1016/j.wasman.2016.06.040, URL http://www.sciencedirect.com/science/article/pii/S0956053X16303452.

Thorpe, A. K., and Coauthors, 2020: Methane emissions from underground gas storage in California. *Environ. Res. Lett.*, **15 (4)**, 045 005, doi:10.1088/1748-9326/ab751d, URL https://doi.org/10.1088%2F1748-9326%2Fab751d, publisher: IOP Publishing.

U.S. EPA, 2014: Other Test Method (OTM) 33 and 33A Geospatial Measurement of Air Pollution-Remote Emissions Quantification Direct Assessment (GMAP-REQ-DA). Tech. rep.

van Ulden, A. P., 1978: Simple estimates for vertical diffusion from sources near the ground. *Atmospheric Environment (1967)*, **12 (11)**, 2125–2129, doi:10.1016/0004-6981(78)90167-1, URL http://www.sciencedirect.com/science/article/pii/0004698178901671.

Varon, D. J., D. J. Jacob, J. McKeever, D. Jervis, B. O. A. Durak, Y. Xia, and Y. Huang, 2018: Quantifying methane point sources from fine-scale satellite observations of atmospheric methane plumes. *Atmospheric Measurement Techniques*, **11 (10)**, 5673–5686, doi:https://doi.org/10.5194/amt-11-5673-2018, URL https://www.atmos-meas-tech.net/11/5673/2018/.

Venkatram, A., 1996: An examination of the Pasquill-Gifford-Turner dispersion scheme. *Atmospheric Environment*, **30 (8)**, 1283–1290, doi:10.1016/1352-2310(95)00367-3, URL http://www.sciencedirect.com/science/article/pii/1352231095003673.

Weil, J. C., W. H. Snyder, R. E. Lawson, and M. S. Shipman, 2002: Experiments On Buoyant Plume Dispersion In A Laboratory Convection Tank. *Boundary-Layer Meteorology*, **102 (3)**, 367–414, doi:10.1023/A:1013874816509, URL https://doi.org/10.1023/A:1013874816509.

Weil, J. C., P. P. Sullivan, and C.-H. Moeng, 2004: The Use of Large-Eddy Simulations in Lagrangian Particle Dispersion Models. *Journal of the Atmospheric Sciences; Boston*, **61 (23)**, 2877–2887, URL http://search.proquest.com/docview/236504887/abstract/B3103183B19C4A61PQ/1.

Weil, J. C., P. P. Sullivan, E. G. Patton, and C.-h. Moeng, 2012: Statistical Variability of Dispersion in the Convective Boundary Layer: Ensembles of Simulations and Observations. *Boundary Layer Meteorology; Dordrecht*, **145 (1)**, 185–210, doi:http://dx.doi.org/10.1007/s10546-012-9704-y, URL https://search.proquest.com/docview/1037769697/abstract/554845EBE12C4655PQ/1.

Willis, G. E., and J. W. Deardorff, 1976: A laboratory model of diffusion into the convective planetary boundary layer: DIFFUSION INTO THE BOUNDARY LAYER. *Quarterly Journal of the Royal Meteorological Society*, **102 (432)**, 427–445, doi:10.1002/qj.49710243212, URL http://doi.wiley.com/10.1002/qj.49710243212.

Xue, F., H. Kikumoto, X. Li, and R. Ooka, 2018: Bayesian source term estimation of atmospheric releases in urban areas using LES approach. *Journal of Hazardous Materials*, **349**, doi:10.1016/j.jhazmat.2018.01.050.

LIST OF TABLES

Table 1. Key input parameters and observed values for each simulation.

Case	**SCBL – Coarse**	**SCBL – Moderate**	**SCBL – Fine**	**WCBL – Coarse**	**WCBL – Moderate**	**WCBL – Fine**
Domain Size (Lx, Ly, Lz) [km]	(5, 5, 2)	(5, 5, 2)	(5, 5, 2)	(3, 3, 1)	(3, 3, 1)	(3, 3, 1)
Cell Count (Nx, Ny, Nz)	(96, 96, 96)	(192, 192, 192)	(500, 500, 200)	(96, 96, 96)	(192, 192, 192)	(500, 500, 160)
Horizontal Resolution [m]	52	26	10	31.25	15.625	6.25
First Cell Height [m]	20.8	10.4	3	10.4	5.2	3
Geostrophic Wind (Ug, Vg) [m/s]	3.6	3.6	3.6	10	10	10
Surface Heating [Km/s]	0.24	0.24	0.24	0.1	0.1	0.1
Obukhov Length [m]	-6.1	-5.9	-5.4	-16.0	-14.9	-12.3
Friction Velocity [m/s]	0.29	0.29	0.29	0.46	0.47	0.45
Bottom of Capping Inversion [m]	1050	1050	1050	525	525	525

TABLE 2. PPG observations used in this study.

SCBL			WCBL		
Run	**u* [m/s]**	**L [m]**	**Run**	**u* [m/s]**	**L [m]**
15	0.22	-6.6	2	0.12	-18
16	0.23	-3.3	5	0.37	-29
25	0.19	-5.4	8	0.29	-19
47	0.22	-5.3	9	0.43	-34
48S	0.21	-5.2	12	0.5	-48
			19	0.37	-25

TABLE 3. LES performance in the SCBL.

	Coarse LES		Moderate LES		Fine LES	
	FB (%)	**t-Test**	**FB (%)**	**t-Test**	**FB (%)**	**t-Test**
50 m	78	Reject	56	Reject	38	Reject
100 m	40	Reject	2	Not Reject	15	Not Reject
200 m	-27	Not Reject	4	Not Reject	-3	Not Reject
400 m	-16	Not Reject	8	Not Reject	-7	Not Reject
800 m	4	Not Reject	5	Not Reject	17	Not Reject

Table 4. LES performance in the WCBL.

	Coarse LES		**Moderate LES**		**Fine LES**	
	FB (%)	**t-Test**	**FB (%)**	**t-Test**	**FB (%)**	**t-Test**
50 m	92	Reject	75	Reject	55	Reject
100 m	25	Reject	12	Reject	-26	Reject
200 m	-17	Not Reject	-50	Reject	-58	Reject
400 m	-48	Reject	-93	Reject	-115	Reject
800 m	-65	Reject	-107	Reject	-138	Reject

	SCBL			WCBL		
	FAC2 (%)	**FB (%)**	**NMSE (%)**	**FAC2 (%)**	**FB (%)**	**NMSE (%)**
50 m	100	3	2	100	4	1
100 m	100	6	5	100	26	7
200 m	100	3	10	100	19	5
400 m	100	-2	7	100	15	5
800 m	60	18	3	83	23	14

Table A1. Performance of SLS theory relative to PPG observations.

LIST OF FIGURES

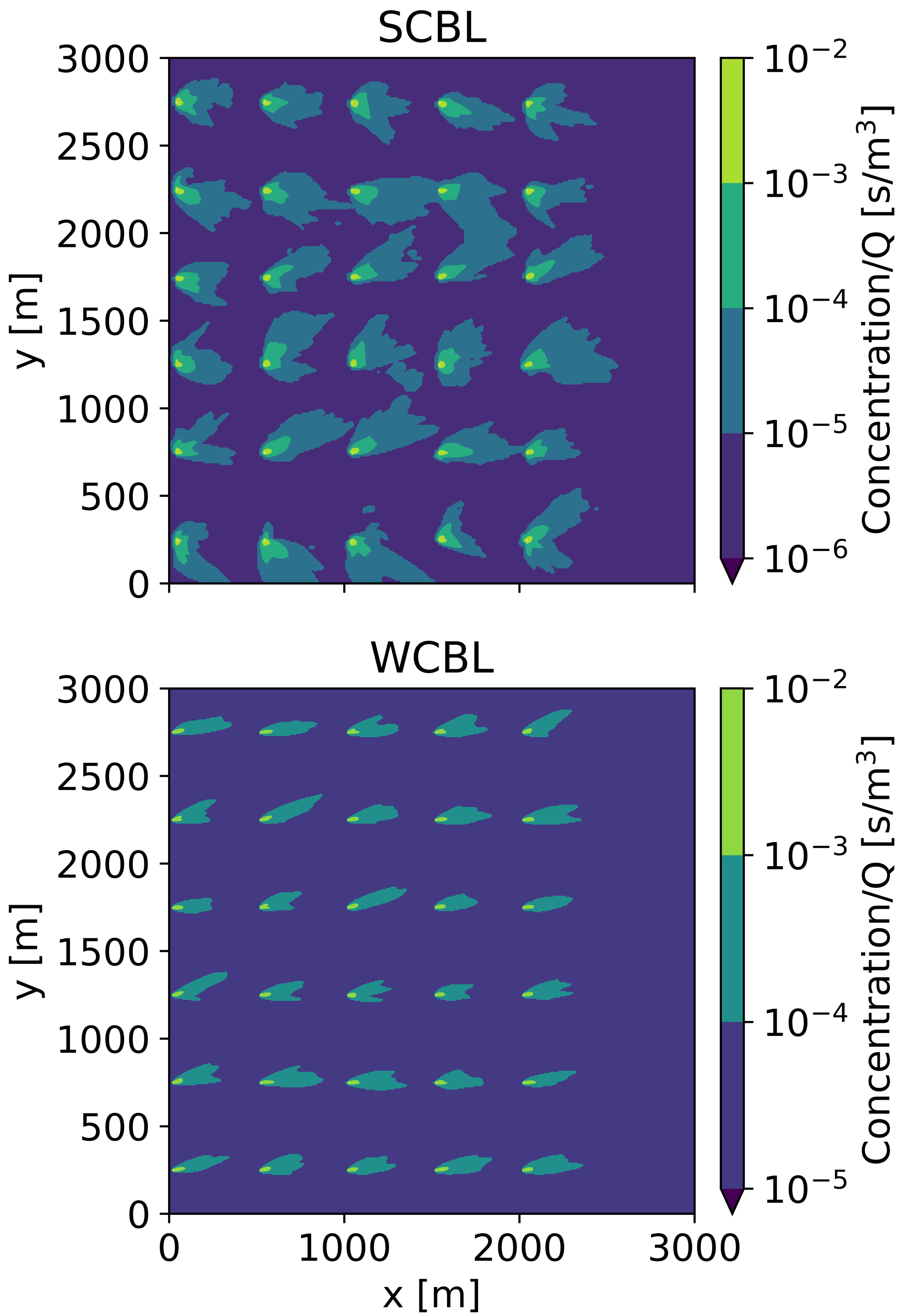

Fig. 1. Grid of normalized 10-minute averaged plume concentrations at 1.5 m within the SCBL and WCBL.

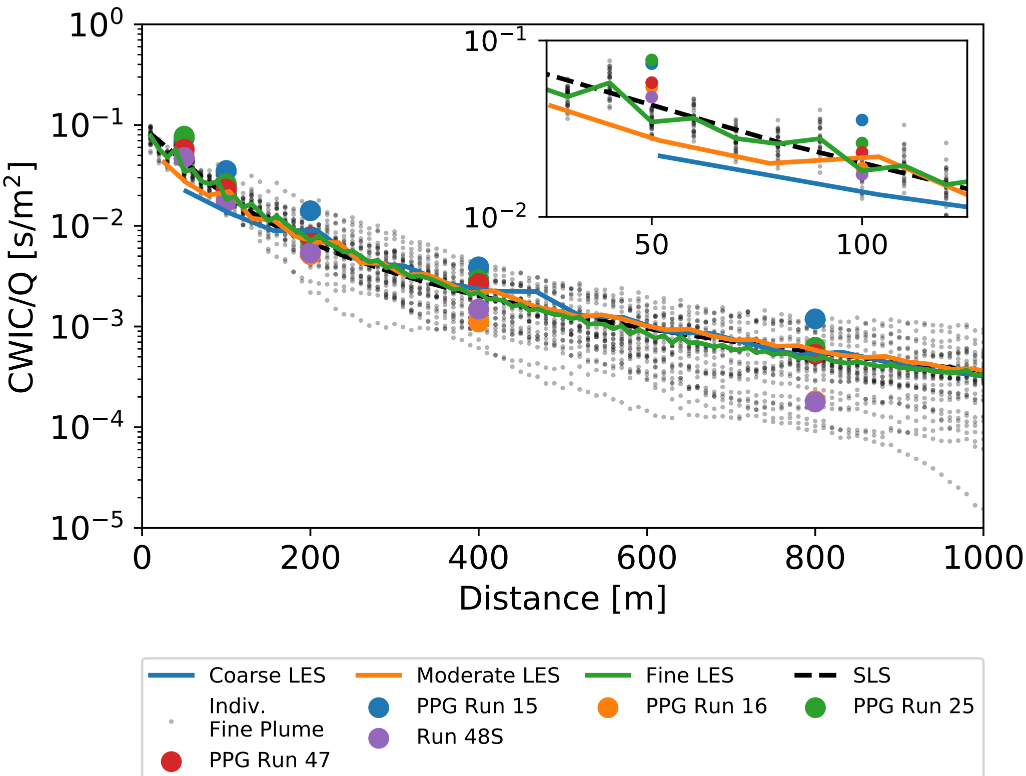

673 FIG. 2. SCBL observations and model predictions for the horizontal array. Ensemble average LES concentrations are shown as solid lines. SLS concentrations are calculated for L=-6 m, u_*=0.29 m s^{-1}.

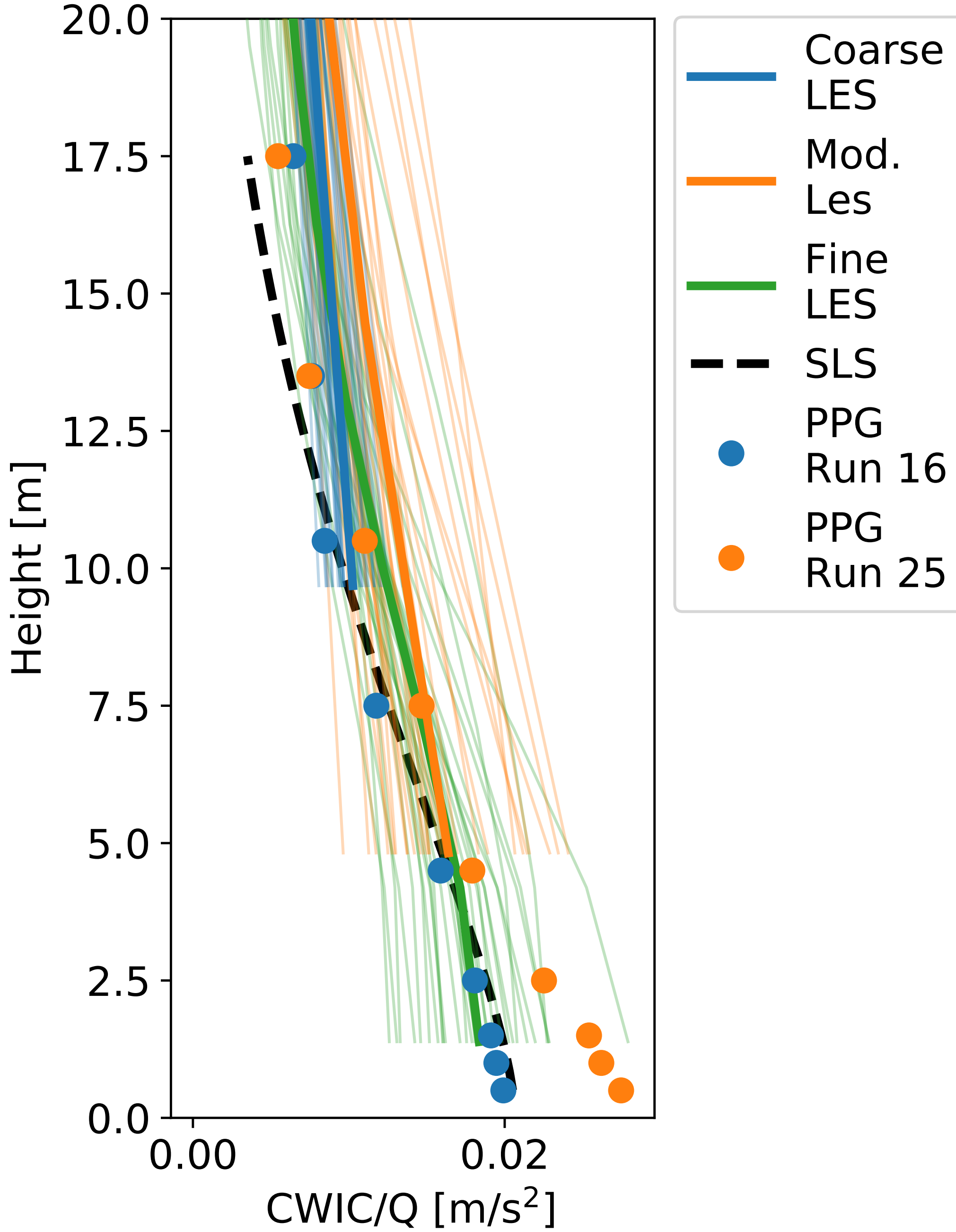

675 FIG. 3. SCBL observations and model predictions for the vertical array at 100-m downwind distance. Ensemble
676 average LES concentrations are shown as solid lines, and individual plumes are shown as thin lines. SLS
677 concentrations are calculated for L=-6 m, u_*=0.2 m s^{-1}.

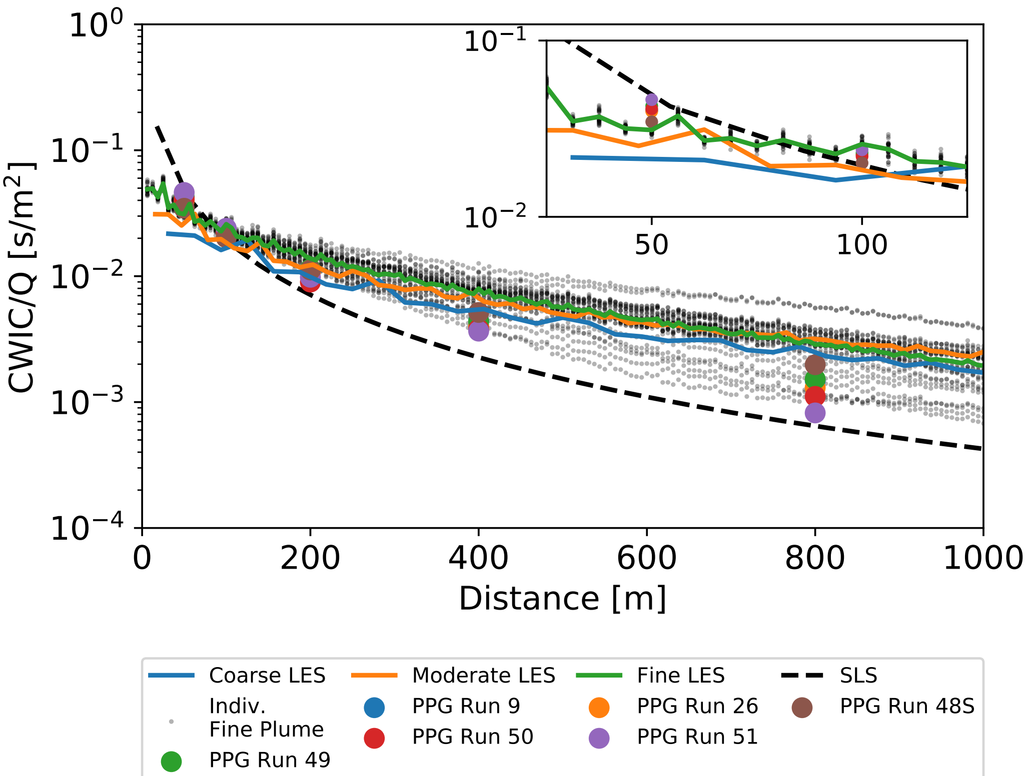

678 FIG. 4. WCBL observations and model predictions for the horizontal array. Ensemble average LES concentrations are shown as solid lines. SLS concentrations are calculated for L=-15 m, u_*=0.45 m s^{-1}.

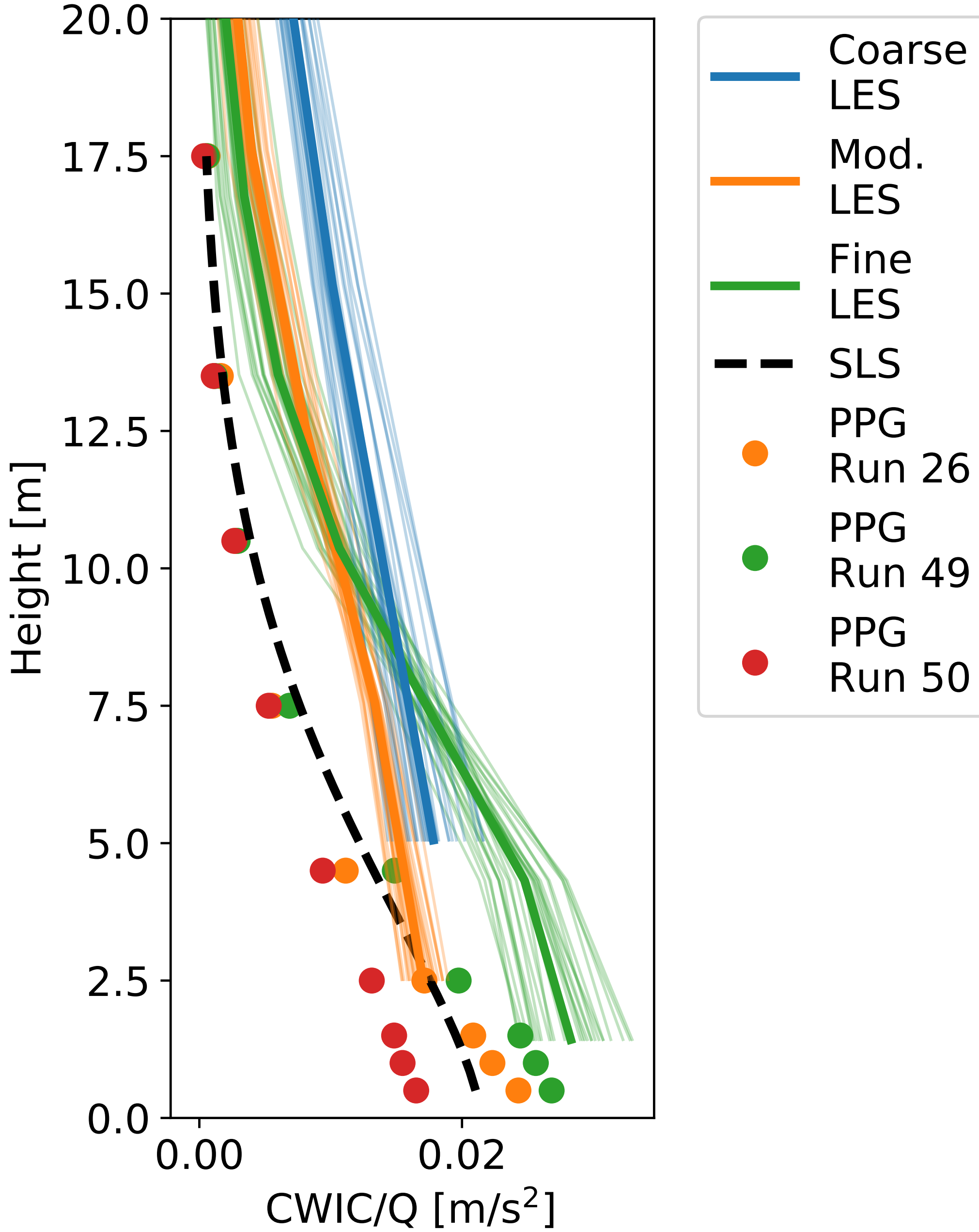

680 FIG. 5. WCBL observations and model predictions for the vertical array at 100-m downwind distance.
681 Ensemble average LES concentrations are shown as solid lines, and individual plumes are shown as thin lines.
682 SLS concentrations are calculated for L=-15 m, u_*=0.45 m s^{-1}.

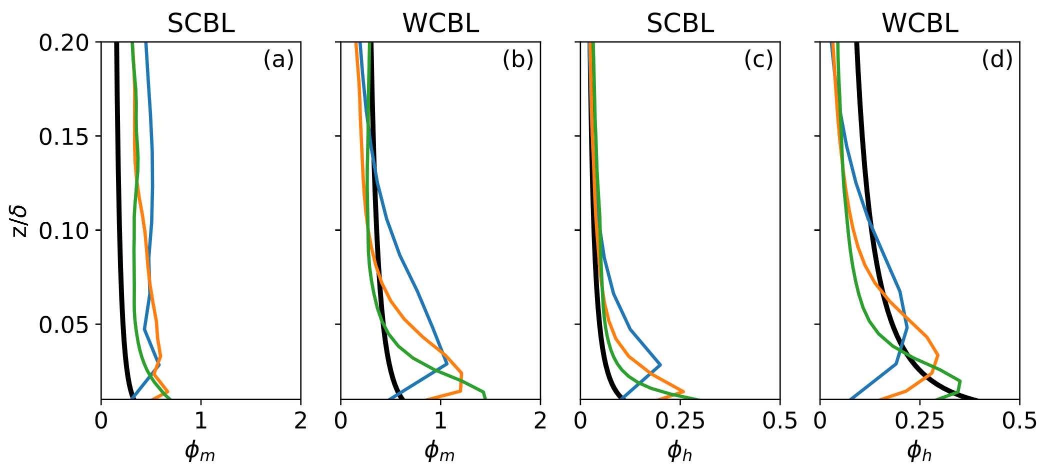

683 FIG. 6. Non-dimensional wind shear ϕ_m (a,b) and temperature gradient ϕ_h (c,d) profiles computed from LES (colored lines) and empirical fits (black line), scaled by boundary layer depth δ, where δ = 1025 m in the SCBL and δ = 525 m in the WCBL.